Colloids and Surfaces B: Biointerfaces 123 (2014) 158–169

Contents lists available at ScienceDirect

Colloids and Surfaces B: Biointerfaces

journal homepage: www.elsevier.com/locate/colsurfb

Synthesis and characterization of $CaCO_3$–biopolymer hybrid nanoporous microparticles for controlled release of doxorubicin

Valeria E. Bosio[a], Maximiliano L. Cacicedo[a], Brice Calvignac[b], Ignacio León[c], Thomas Beuvier[d], Frank Boury[b], Guillermo R. Castro[a,*]

[a] Nanobiomaterials Laboratory, Institute of Applied Biotechnology (CINDEFI, CONICET-UNLP, CCT La Plata), Dept. of Chemistry, School of Sciences, Universidad Nacional de La Plata, Calle 47 y 115, CP 1900 La Plata, Argentina
[b] LUNAM, Université d'Angers, UMR S-1066, Micro-Nanomédecines Biomimétiques, IBS Institut de Biologie en Santé, Batiment IRIS, 4 rue Larrey, 49933 Angers Cedex 9, France
[c] Chemical Inorganic Center (CEQUINOR, CONICET CCT La Plata) – School of Sciences – Universidad Nacional de La Plata (UNLP), La Plata CP 1900, Argentina
[d] LUNAM, Université du Maine, Institut des Molécules et Matériaux du Mans, UMR CNRS 6283, Avenue Olivier Messiaen, 72085 Le Mans Cedex 9, France

ARTICLE INFO

Article history:
Received 25 February 2014
Received in revised form 1 August 2014
Accepted 4 September 2014
Available online 16 September 2014

Keywords:
Hybrid microparticles
Doxorubicin
Drug delivery
Cancer therapy
Nanoporous
Cell targeting

ABSTRACT

Doxorubicin (Dox) is a hydrophilic drug extensively used for treatment of breast, lung, and ovarian cancer, among others; it is highly toxic and can cause serious side effects on nontargeted tissues. We developed and studied a hybrid nanoporous microparticle (hNP) carrier based on calcium carbonate and biopolymers derivatized with folic acid (FA) and containing Dox as a chemotherapeutic drug model. The hNPs were characterized by X-ray diffraction, and Raman and Fourier transform infrared (FTIR) spectroscopies. The X-ray diffraction patterns of calcium carbonate particles showed about 30–70% vaterite–calcite polymorphisms and up to 95% vaterite, depending on the absence or the presence of biopolymers as well as their type. Scanning electron microcopy images revealed that all types of hNPs were approximately spherical and porous with average diameter 1–5 μm, and smaller than $CaCO_3$ microparticles. The presence of biopolymers in the matrices was confirmed after derivatization with a fluorescein isothiocyanate probe by means of confocal microscopy and FTIR synchrotron beamline analysis. In addition, the coupling of lambda carrageenan (λ-Car) to FA in the microparticles (FA–λ-Car-hNPs) increased the cancer-cell targeting and also extended the specific surface area by up to ninefold (26.6 $m^2 g^{-1}$), as determined by the Brunauer–Emmett–Teller isotherm. A nanostructured porous surface was found in all instances, and the FA–λ-Car-hNP pore size was about 30 nm, as calculated by means of the Barrett–Joyner–Halenda adsorption average. The test of FA–λ-Car-hNP anticancer activity on human osteosarcoma MG-63 cell line showed cell viabilities of 13% and 100% with and without Dox, respectively, as determined by crystal violet staining after 24 h of incubation.

1. Introduction

Micro- and nanomedicines for the treatment of life-threatening diseases such as cancer, AIDS, diabetes, malaria, prion infection, and tuberculosis are in different phases of clinical trials for approval, though some are already currently in use in palliative therapies. Several drugs and/or bioactive molecules have been successfully encapsulated in order to improve bioavailability, bioactivity, and delivery control [1,2]. Drug encapsulation offers the advantages of drug protection against a degradative physiological process, reduction in the potential toxic side effects associated with the drug dosage, increase in patient comfort by avoiding repetitive bolus injections or the use of perfusion pumps, and favorable drug pharmacokinetics. However, drug formulations depend on the choice of suitable carriers that must possess high encapsulation efficiency, improved bioavailability, a specified drug-retention time, lengthy stability, and no toxicity, among other relevant properties. Generally, most micro- and nanomedicines are formulated by a trial-and-error method but with only minimum rational design. In addition, since the usual procedure for making drug formulations is generally based solely on a consideration of the interactions of the cargo molecule and/or the vehicle matrix with the target tissues without taking into account the mutual physicochemical reactions between those pharmacologic components, this approach is hampered by serious limitations for therapeutic use. Advanced

* Corresponding author. Tel.: +54 221 483 37 94x132/103; fax: +54 221 483 37 94x132/103.
E-mail address: grcastro@gmail.com (G.R. Castro).

http://dx.doi.org/10.1016/j.colsurfb.2014.09.011
0927-7765/

developments in drug micro- and nano-formulations must consider ways to control the kinetic release of the cargo; interactions among the drug, the matrix, and the other major components of the admixture; the effects of the environment on the formulation; and drug stability and toxicity, among other issues. Furthermore, the new capabilities of these recently developed medicines are also influenced by particle size, surface charge, the presence of specific chemical functional groups, and the distribution and ratio of hydrophobic and hydrophilic regions in the carrier [1–5].

Controlled drug delivery is today one of the most challenging therapeutic strategies for the treatment of acute and chronic pathologies. Among the different strategies for the development of drug delivery matrices, biopolymers represent an attractive alternative to take into account because of remarkable properties, such as great diversity in chemical structure, stereospecific functionality, a defined and wide range of molecular weight, biologic features, virtual lack of toxic side effects, and also because they can be considered as green technology [2,4,5]. In addition, natural polymers offer significant advantages over chemically synthesized ones because of their low production and purification costs, easy tailoring, and degradability, along with the use of soft conditions for cross-linking. Moreover, some polymers such as alginates, carrageenans, pectins and other polysaccharides are considered as GRAS (generally recognized as safe) by the Food and Drug Administration (FDA, US) and thus are extensively used in the food industry. These reasons converge to consider biopolymers as one of the most promising materials for the environmentally compatible synthesis of micro- and nanodrug carriers. Polymer-based-particle synthesis can be categorized according to four basic mechanisms: covalent cross-linking, ionotropic cross-linking, polyelectrolyte complexation, and self-assembly [1,2,4].

Pectins (Pecs) are heteropolysaccharides extracted from plant cell walls used in many applications as a thickener or gelling agent in the food industry. Pecs are composed of linear polysaccharides of partially methoxylated poly[alpha-(1,4)-D-galacturonic acids] with pendant rhamnogalacturonan units (heteropolymer of repeating [1 → 2]α-L-rhamnosyl-[l-L]α-D-galactosyluronic acid disaccharide units). Pecs can be grouped into low-methoxylated pectin (LMP) with an esterification degree (ED) below 40%, medium-methoxylated pectin (MMP) with an ED range between 40% and 60%, and high-methoxylated pectin (HMP) with an ED higher than 60%. LMP and MMP can be gelled by multivalent cations, while HMP only at acid pH and in the presence of solutes. Pecs with an esterification degree between 20% and 75% are able to form gels by an ionotropic mechanism of polymer interchain cross-linking mediated by multivalent cations. Interestingly, Pec hydrogels are temperature- and pH-sensitive, which is structurally associated with the simultaneous presence of hydrophilic/hydrophobic motifs in the polymer. Particularly, the strength of Pec-gels is enhanced by lowering the environmental pH and/or temperature, allowing them to be classified as smart biogels [5]. Also, Pec anti-adhesive and apoptosis-inducing activities in cancer cells were recently reviewed [6]. The potential anticancer activities combined with the environmental gel sensitivity make Pec gels interesting models for the development of new drug delivery hydrogel matrices combined with anticancer drugs.

Carrageenans (Cars) are a family of linear sulfated polygalactans extracted from marine red algae. Cars are currently used as a thickener or as gelling agents and also as emulsifier and stabilizer polymers in the food and pharmaceutical industries. Cars are chemically composed of alternate D-galactose and 3,6-anhydrogalactose monomers linked by α-1,3 and β-1,4-glycosidic bonds and sulfated at up to 41% (w/w). Cars are generally classified on the basis of their solubility on KCl aqueous solutions which depends on the numbers and positions of ester sulfate and 3,6-anhydrogalactose monomers. The kappa (κ), iota (ι) and lambda (λ)-Car dimers typically have one, two and three sulfate ester groups with an average content of 20%, 33% and 38% (w/w), respectively. Kappa and iota Cars form thermoreversible gels but only the first one can exhibit syneresis. Also, both Car polymers are able to form gels in the presence of potassium or calcium ions. However, lambda-Car is not able to form gels, but is soluble in cold water making viscous solutions typically from 60 to 300 mPa s. Biological activities of Cars include induction of inflammatory process but also antitumor, immunomodulatory, antiviral and anticoagulant activities [7].

The processes to develop biopolymer matrices by ionotropic cross-linking have been under study for a long time, and now some of them are in the market. During the gelling polymer process and in the presence of appropriate counterions, it is possible to synthesize insoluble salts to make hybrid systems. Biomineralization allows the development of artificial hybrid materials with novel and remarkable properties. Besides, the presence of hybrid materials in living organisms with different evolution levels is a typical example of nature's complexity and functionality. Among the most abundant inorganic materials in nature, calcium carbonate plays a major role and it can be found in pearls, and mollusk shells as a result of biomineralization mechanisms. Aragonite, calcite and vaterite are the most common crystalline structures of $CaCO_3$ in living organisms. Vaterite is the most stable and useful polymorphism for making microparticles because of its crystal size, distribution, and spherical geometry [8]. Interestingly, several strategies for synthetizing different $CaCO_3$ crystal structures and morphologies in the presence of biopolymers such as starch, kappa (κ) and iota (ι) carrageenans, collagen, dextrans, and alginates were previously reported [9–12]. The advantages of controlling the self-assembly and precise manipulation of $CaCO_3$ hybrid systems by biopolymer templates to synthetize matrices with distinctive architectures and sensitivities to the environmental conditions have attracted attention for the development of molecular loading and delivery devices [13,14].

Anthracyclines, such as doxorubicin, are one of the most therapeutic molecules employed in the treatment of cancer. However, these compounds can cause undesirable side effects on nontargeted organs (*e.g.*, heart, liver, kidneys, stomach, and blood-cell lineages) along with unwanted physiologic consequences during long-term or repeated treatments such as lengthy chemotherapies or recurrent pathologies. Doxorubicin hydrochloride (Dox) is commonly used in the treatment of many solid tumors, such as breast, lung, stomach, or ovarian carcinoma and sarcomas [15]. Dox inhibits cell growth by DNA intercalation and inhibition of topoisomerase II along with various actions on cell metabolism. Unfortunately, Dox is highly toxic, and the biodistribution of anthracycline to nontargeted tissues causes serious side effects that limit its dosage and use. Therefore, the development of new formulation strategies involving Dox encapsulated in particulate drug delivery systems would be highly desirable. Many studies carried out with anthracyclines have given rise to a variety of Dox-containing micro- and nanoparticles such as polymeric carriers, inorganic magnetic nanoparticles with surface-adsorbed Dox, or even solid lipid nanoparticles incorporating Dox through ion-pair complex formation [15]. Particularly, the synthesis of $CaCO_3$ particles, nanocomposites made of carboxymethyl cellulose-$CaCO_3$ and carbonate-apatite for transport of Dox has recently been reported for the treatment of colon cancer and osteosarcomas [16–18].

Since Dox is a hydrophilic and water-soluble molecule, the encapsulation of anthracycline into micro- and/or nanoparticulate systems at a high rate and yield – and with a long shelf-life and well controlled kinetic release – ultimately remains as the main challenge. In addition, major difficulties arise in controlling the cargo release, while within the formulation process a compromise must be found between encapsulation efficiency and the drug leakage

induced by diffusion and/or matrix degradation as well as between the biocompatibility and biodegradation of particle components.

In our previous work, the development and characterization of biogel microbeads composed of alginate and carboxymethylated guar gum to encapsulate Dox in the presence of Congo Red as a molecular helper was analyzed [19]. The strategy was to use the hydrophobic aromatic ring of the polar Dox molecule interacting with the planar aromatic ring structure of the CR, a phenomenon commonly described as π–π stacking. The results showed that the amount of CR was able to control Dox loading into the matrix and also the kinetics of drug release [19]. In the present work, the approach was to encapsulate Dox in a matrix but using the opposite strategy: hydrophilic interactions. In this sense, a selected biopolymer was chemically modified with a polar molecule, folic acid (FA), with the advantage of adding two additional carboxylic groups per FA molecule incorporated in the polymer chain. Another advantage is that FA is a well-known cellular marker and the FA-receptor expression is enhanced on most of the cancer-cell surface. Accordingly, decoration of biopolymer-containing microsphere surfaces with FA should effectively increase the targeting of Dox to most of cancer cells and concomitantly reduce the high toxic side effects of the anthracycline.

The aim of the present work was therefore to develop, tailor and characterize hybrid nanostructured microparticles (hNPs) based on an inorganic-hydrogel matrix designed to deliver Dox as a chemotherapeutic agent to target cancer cells. The hybrid microparticles containing Dox were analyzed by optical, fluorescence, confocal and scanning electron microscopies, FTIR, Raman and X-ray diffraction spectroscopies, porosity determination by nitrogen adsorption isotherms, loading and release studies *in vitro*. Also, the behavior of the hybrid microparticles in NIH 3T3 and MG-63 cell cultures are reported.

2. Materials and methods

2.1. Chemicals and media

The biopolymers used in the present work were: kappa and iota carrageenans (κ-Car and ι-Car) from Satiagel (SKW Biosystems). Dox was kindly supplied by LMK pharmaceuticals (Argentina). All the other reagents used were of analytical grade and purchased from Sigma–Aldrich (St. Louis, MO, USA) or Merck (Darmstadt, Germany) except when otherwise specified.

Dox was quantified by spectrofluorimetry (Perkin Elmer LS 50B, Japan) at a λ_{exc} of 454 nm and a λ_{em} of 588 nm through the use of the appropriate calibration curve [5].

All the biopolymer and formulation solutions were made in MilliQ water (Millipore, Billerica, USA). The Dox stock solutions (0.9 g/l) and their dilutions were made in either MilliQ water or buffers as stated.

Cell culture materials were purchased from Trading New Technologies (Buenos Aires, Argentina). Dulbecco's Modified Eagle's Minimal Essential Medium (DMEM) and fetal bovine serum (FBS) were supplied by GBO (Buenos Aires, Argentina), while trypsin-EDTA was provided by Gibco (Gaithersburg, MD, USA).

2.2. Dox–biopolymer interactions

Aqueous solutions of 1.0% (w/v) Pecs and Cars were made in MilliQ™ water (Millipore, Billerica, MA, USA) supplemented with 10 μM sodium azide and kept at 5 °C until use. After incubating 375 μl of the biopolymer stock solutions with 125 μl of Dox solution for 2 h and 15 min at 25 °C, 1.0 ml of chilled acetone or ethanol was added to precipitate the biopolymer–cargo molecule complex, followed by sedimentation at 10,000 × *g* for 5 min. The Dox concentration was measured in the supernatant by spectrofluorometry as cited above.

2.3. Biopolymer targeting

2.3.1. Fluorescein isothiocyanate-labeled biopolymer

The derivatization of selected biopolymers with the fluorescein isothiocyanate (FITC) probe was performed as previously described [20].

2.3.2. Folic-acid targeted λ-Car

The FA was coupled to λ-Car by an initial carboxymethylation of the λ-Car and a subsequent activation by addition of the carbodiimide (CDI) reactive group. The protocols for the carboxymethylation of λ-Car, the formation of the carboxymethyl Car (CM-Car) CDI derivative, and the coupling of (CDI-CM)-λ-Car to FA have been previously described [20,21].

2.4. The hNP synthesis

Biopolymer microparticles were synthesized in glass vials by colloidal crystallization with $CaCl_2$ in the presence of Glycine (Gly, Sigma–Aldrich, Saint-Quentin-Fallavier, France), NaCl (VWR International, Fontenay-sous-Bois, France), Na_2CO_3, and one of the following polymers: hyaluronic acid, λ-, κ-, or ι-Car. An aqueous solution of 3.2% (w/v) $CaCl_2$ in 1.25 M Gly–NaCl buffer (pH 10.0) was prepared and kept frozen until use. During preparation, the pH of the solution was adjusted to the desired value with NaOH or HCl. A 3.2% (w/v) Na_2CO_3 solution was prepared in MilliQ™ water and used immediately.

In a typical experiment, 9.0 ml of a 3.2% (w/v) Na_2CO_3 solution was mixed with 2.0 ml of 1.0% (w/v) biopolymer solution in a 50-ml Falcon tube under stirring (1000 rpm) for 1 min in an ice bath. Then 9.0 ml of 3.2% (w/v) $CaCl_2$ in the Gly buffer was added and mixed with stirring for 5 min. The final concentrations in the reaction mixture were, therefore, 0.1% (w/v) for each biopolymer and 1.6% (w/v) for the Ca^{2+} and CO_3^{2-} ions. MilliQ™ water was then added to a final volume of 30 ml and the precipitated $CaCO_3$–biopolymer products were collected by centrifugation. The precipitate was washed with 30 ml of MilliQ™ water by centrifugation, and the pellet was frozen in liquid N_2 before lyophilization and final storage under vacuum in a desiccator at room temperature until the time of characterization.

2.5. Characterization of the hNP

2.5.1. Optical and fluorescence microscopy

Optical and fluorescence microscopy was carried out with a Leica DM 2500 microscope (Wetzlar, Germany) equipped with a UV source and filters (495–505 nm) for fluorescence observation.

2.5.2. Confocal laser scanning microscopy (CLSM)

FITC-labeled and non-labeled biopolymer microparticles were examined in a Zeiss LSM 510 confocal microscope (Oberkochen, Germany). The microscope collected 12-bit images at different overlapping planes (scan-mode plane) with four detectors for fluorescent signals and a transmission detector for bright-field images. These images were then superimposed electronically in correct registration to give the final composite image (the merge). The microscope has four lasers with multiple laser lines for excitation of fluorophores (*via* the FITC filter). The software LSM 510 (2.01 v.) was used for operating the microscope, for the merge, and for data analysis.

2.5.3. Scanning electron microscopy

Scanning electron microscopy (SEM) images (JEOL 6310F, Croissy-sur-Seine, France) were obtained with a tungsten cathode field emission gun operated at 3.0 kV on dispersed powder in adhesive carbon supports. The samples were prepared by sputtering the surface with gold by means of a metallizer (Balzers SCD 030) to obtain a layer thickness between 15 and 20 nm. The morphologies and surface features of the microspheres were also observed in a Philips SEM Model 505 scanning electron microscope (Rochester, NY, USA), and processed by an image digitizer program (Soft Imaging System ADDA II, SIS).

2.5.4. Roughness analysis

SEM images were analyzed by ImageJ software (NIH, USA). The roughness of the surface was reflected in the standard variation of the gray values of all the pixels on the image (at 2000×). First, the SEM image file was opened by the software and converted to an 8-bit image. Then all the pixels on the image were selected and statistically measured by the computer. The lower the standard-variation value was, the smoother the surface was shown to be. Histograms of the SEM images at 3000× magnification were finally performed in duplicate.

2.5.5. X-ray diffraction

X-ray diffraction patterns for the different formulations spread over a glass substrate were collected in reflection mode on powder and analyzed by the *Origin* program. The measurement was performed with an X-pert^{TM} diffractometer using Cu-Kα radiation (λ = 1.54056 Å) from $2\theta = 10^{\circ}$ to 70° in continuous mode with a 0.07° step size.

2.5.6. Vibrational analysis: FTIR and Raman spectroscopy

The λ-Car and λ-Car–Dox complexes were analyzed by FTIR (JASCO FTIR-4200, Japan). Pellets were prepared by mortaring the samples at 5.0% (w/w) with KBr (Pike Technologies, Madison, USA) and scanning with background correction at 256 scans with a high-energy ceramic source and a DLATGS (deuterated L-alanine-doped triglicine sulfate) detector with final analysis by the *Origin* program. FTIR scans were recorded in the 4000–400 cm^{-1} range at 4 cm^{-1} resolution. In addition, the hNP-Dox formulations with and without FA were determined by FTIR at the SMIS (Soleil, French National Synchrotron Facility, France) beamline and the results were drawn and analyzed by the *Omnic* software. Images of Dox fluorescence in the hNPs were furthermore obtained for the same samples.

The microscopic observation and Raman-spectra generation were carried out with a Nikon microscope linked to a Raman FRA 106 accessory of a FTIR Bruker 66 (Billerica, MA, USA). The samples were analyzed under a 50X objective (focal distance, 12 mm) upon irradiation with a 514 nm Nd-YAG Perkin-Elmer laser.

2.5.7. Nitrogen adsorption isotherms

Nitrogen adsorption–desorption at 77 K at a bath temperature of −195.8 °C was carried out for dry microparticles. The surface area, pore volume and pore size of the different formulations were calculated with Micromeritics ASAP 2020 V3.00 Software considering the Brunauer–Emmett–Teller (BET) equation or the Barrett–Joyner–Halenda (BJH) method.

2.5.8. Car molecular weight determination

The three different Cars were studied by a high-pressure size-exclusion chromatography system coupled to a refractometer. Polymer solutions at usually 2.0 mg/ml were solubilized in MilliQ^{TM} water and then filtered through 0.45-μm pore diameter filters. The filtered polymer was injected onto a PL-Aquagel-OH (Varian) column equilibrated with 100 mM ammonium acetate. The recovery index was calculated by the software and the concentration determined by refractometry after the appropriate calibration (Supplementary material, Table 1S).

2.6. Dox loading and release studies

Dox-loaded microparticles were prepared by the adsorption method. Weighed dehydrated hNPs (10, 25, or 50 mg) were suspended in 500 μl of MES [2-(N-morpholino)ethanesulfonic acid] buffer (pH 6.5). The Dox stock solution was then added to a final concentration of 2.0 mg/ml. The microspheres were incubated under a constant stirring of 30 rpm at 4 °C for 6 h. Next, the microparticles were pelleted and washed by centrifuging two times with MilliQ^{TM} water.

The residual Dox in the supernatants was assayed spectrofluorometrically as mentioned above after loading and two washings with the loading buffer. The loading efficiency (LE) was evaluated as follows:

$$EE_{Dox} = \frac{(Dox)_{to} - (Dox)_{sup}}{(Dox)_{to}} \quad (1)$$

where EE_{Dox} is the entrapment efficiency defined as the difference between the Dox concentration at time zero and in the supernatant, divided by the concentration at time zero.

The pellets containing the centrifuged microspheres were lyophilized and stored until the time of assay. For the release experiments, 10.0–50.0 mg of dehydrated microspheres plus 1.5 ml of buffer were placed in a 2.0-ml Reacti-road^{TM} flask, and Dox release was performed at 37 °C and 30 rpm. At specific intervals, 300-μl samples were withdrawn and replaced with an equal volume of fresh buffer. The Dox concentration upon release was determined by fluorescence as mentioned above.

2.7. Cell cultures

Cell lines not expressing folic acid receptors MG-63 and NIH 3T3 were selected for the studies with hybrid microparticles.

The MG-63 osteoblastic human osteosarcoma-derived cell line (ATCC CRL-1427) was grown in DMEM supplemented with 100 U/ml penicillin, 100 μg/ml streptomycin, and 10% (v/v) fetal bovine serum (FBS) at 37 °C under an atmosphere of 5% (v/v) CO_2 in air. Cultures reaching 100% confluence were subcultured by treatment with 0.1% (w/v) trypsin plus 1.0 mM EDTA in Ca^{2+}/Mg^{2+}-free phosphate-buffered saline (PBS: 11 mM KH_2PO_4, 26 mM Na_2HPO_4, 115 mM NaCl, pH 7.4). For the experiments, the cells (3×10^4 cells/ml) were grown in 48-well plates at 37 °C for 24 h. Then, the resulting monolayer was incubated with different concentrations of the samples for the proliferation assay.

NIH-3T3 mouse fibroblast cells (CRL-1658^{TM}), obtained from the American Type Culture Collection (Manassas, VA, USA), were routinely seeded at 5000 cells per well (400 μl, 1.9 cm^2) in 24-well plates and grown in DMEM with 10% (v/v) heat-inactivated FBS plus the above antibiotics at 37 °C and 5% CO_2 in air.

2.8. Cell culture studies

The hNP anticancer activity, as assessed by loss of cell viability, was tested with the MG-63 cells by the crystal violet assay. Polystyrene particles of 5-μm diameter were used as a control for the evaluation of the NIH-3T3 fibroblast cytotoxicity.

2.9. Viability determination (crystal violet assay)

The bioassay for mitogenesis was carried out as previously reported with certain modifications [22]. Stated in brief, after growth in 48-well plates for 24 h, cultures were incubated with

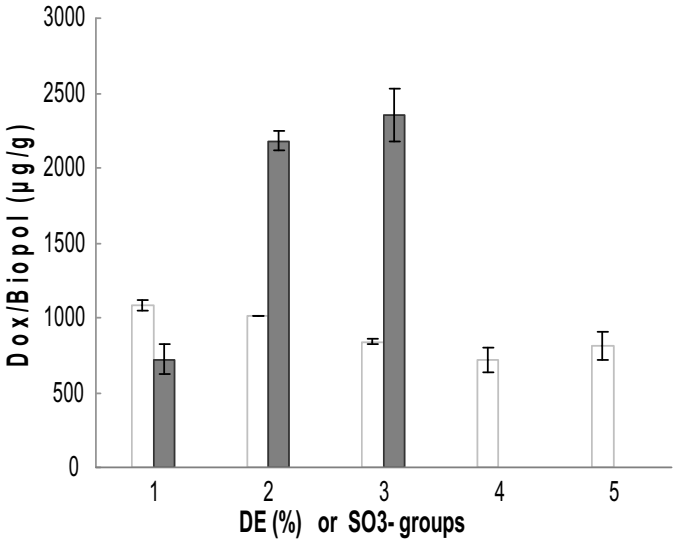

Fig. 1. Dox-biopolymer complexes after 2-h incubation: pectins with different methylation degrees (white bars, left to right: 33.0; 35.4; 55.3; 67.2 and 74.0%) and carrageenins: (gray bars, left to right: with one SO_3^- group or κ-Car; two SO_3^- groups or ι-Car and three SO_3^- groups or λ-Car). Errors bars represent the dispersion of the mean of at least three independent experiments.

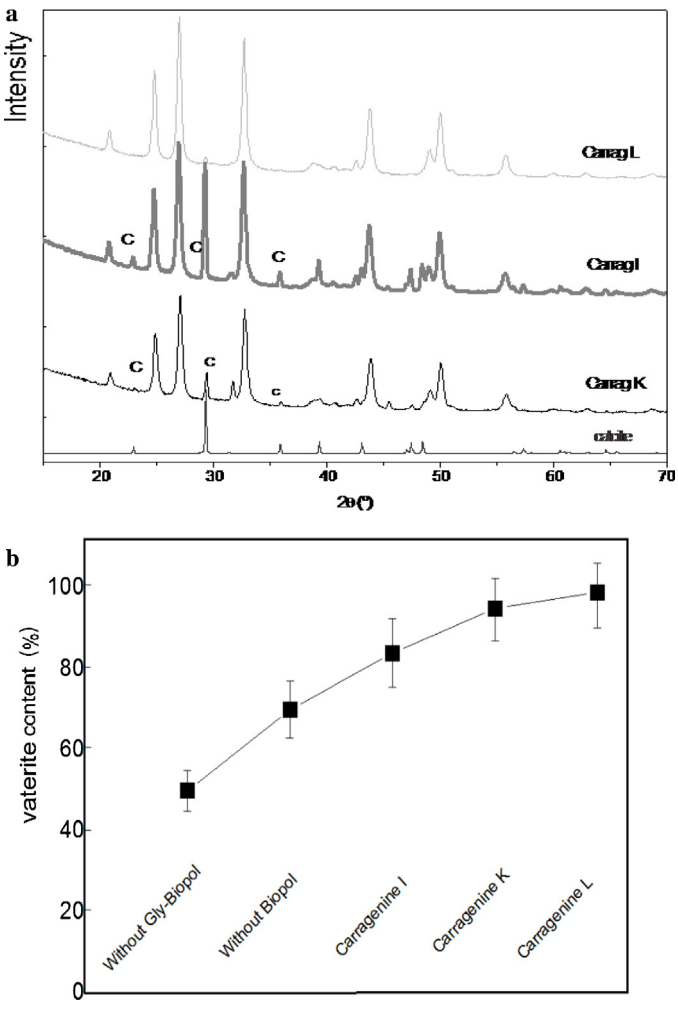

Fig. 2. (a) X-ray diffractogram of $CaCO_3$ (vaterite) in absence and presence of κ, ι I and λ carrageenans. Symbol: C, calcite. (b) Vaterite content in NhPs made in absence or presence of K, I and L carrageenins and Gly buffer. The values are the mean of three replicates ($n = 3$) with standard deviation (SD ≤ 10%). Comparisons of the means were performed by analysis of variance (ANOVA) with a significance level of 5.0% ($p < 0.05$) followed by Fisher's test at $p < 0.05$.

different supernatants collected from the Dox-release assays of the hNP systems under simulated physiologic conditions at various time points; alternatively the cells were exposed directly to the different concentrations of hNPs with and without the loaded Dox as controls (Fig. 9). Then the monolayers were washed with PBS and fixed with 5% glutaraldehyde in PBS at room temperature for 10 min. Finally, for staining, the plates were treated with 0.5% (w/v) crystal violet in 25% (v/v) aqueous methanol for 10 min, then washed with water and dried. The dye taken up by the cells was extracted with 0.5 ml of 30% (v/v) methanol in 100 mM Gly–HCl buffer (pH, 3.0) per well and transferred to test tubes. Absorbance was read spectrophotometrically at 540 nm after an appropriate sample dilution. We have previously shown that under these conditions the colorimetric bioassay strongly correlated with the cell proliferation measured by cell counting in a Neubauer chamber [23,24].

2.10. Statistical methods

At least three independent experiments were performed under each condition. The results are expressed as a percentage and represented by the mean ± SEM (always less than 6.6%). Differences among the data were assessed for statistical significance by analysis of variance (ANOVA).

3. Results and discussion

3.1. Screening for biopolymer synthesis template

Thirteen biopolymers-three Cars, three chitosans, hyaluronic acid, five Pecs, and xylan-were screened as potential matrices for Dox loading as previously reported [5]. Cars and Pecs were selected for further binding studies because of the high interaction with the anthracycline (data not shown). Different sulfonated Cars and Pecs with diverse degrees of esterification were screened with Dox to develop hNP formulations (Fig. 1).

Since the Cars showed better results than the Pecs (Fig. 1), the κ-, ι-, and λ-Cars were selected to develop the hNPs. The Car molecular weights were characterized by high-performance liquid chromatography after the appropriate calibration (Supplemented Material, Table. 1S).

3.2. Inorganic crystallization in the Car matrices

The vaterite content of the crystallization network during the formation of microspheres changed drastically with the type of polymer present in solution, and the crystal structure found could be attributed to the amount of polar groups in the polymers (Fig. 2a). The X-ray-diffraction peaks observed in the figure are characteristic of $CaCO_3$ polymorphism in the form of vaterite. In addition, no peaks at 2θ of 29.3° were observed, indicating the absence of calcite in the microspheres under all the synthesis conditions tested (Fig. 2a) [25]. In order to evaluate the effect of the matrix components on the vaterite content, the percent vaterite present with and without the Gly buffer or the biopolymers was measured. The resulting samples were likewise analyzed by X-ray diffraction (Fig. 2), but also by FTIR and Raman vibrational spectroscopy (data not shown) and SEM (Fig. 3). The presence of the Gly buffer and/or the different biopolymers strongly influenced the vaterite content in the network. For example, a higher value of vaterite (up to 100%) was found for the λ-Car-$CaCO_3$ network than for the hyaluronic acid–$CaCO_3$ hybrid system reported

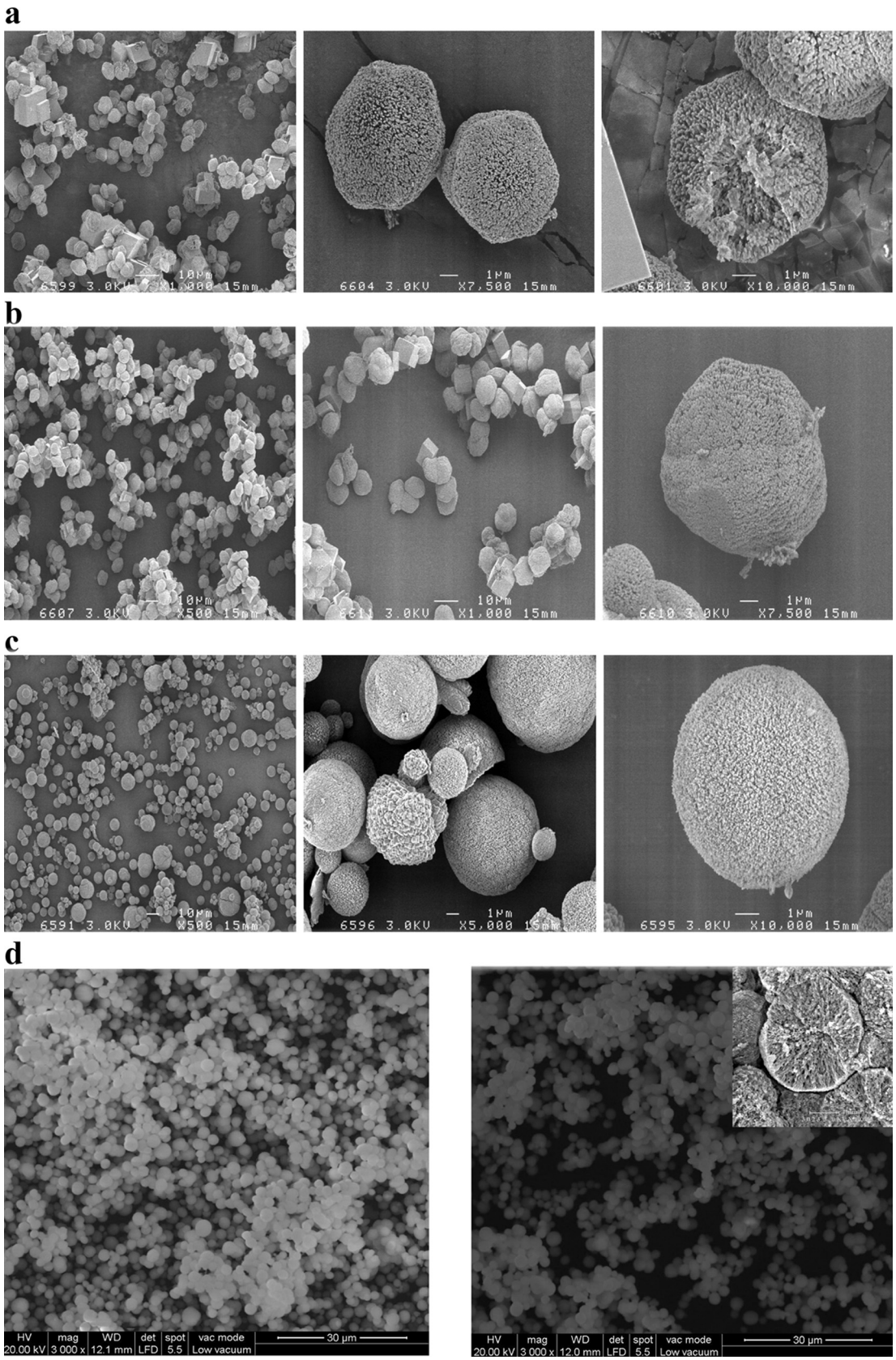

Fig. 3. SEM images of the $CaCO_3$ microparticles synthesized. (a) $CaCO_3$ MP without Gly buffer and without biopolymers. (b) $CaCO_3$ MP without biopolymers. (c) hNPs with biopolymer and (d) optimization of the synthesis for λ-Car and FA–λ-Car (left and right respectively); longitudinal cut particle of FA–λ-Car on the right inset figure.

previously [1]. The phenomena could be explained by the presence of sulfonate groups present in the Cars. The addition of Car to the Na_2CO_3 aqueous solution at the beginning of the synthesis may lead to certain immobilization of carbonate groups in terms of diffusion rates, considering the 0.1% (w/v) λ-Car concentration and the resulting viscosity [11]. Depending on the experimental conditions, *e.g.*, ionic strength and the nature of the ions in the solution, temperature, pH, *etc.*, Car viscosities could reach between 60 and 300 mPa s, which is about 1000 times higher than the viscosity of distilled water [26]. Also, the λ-Car molecules in solution become more ordered at low temperatures and consequently, they show stiffer structures that reduce all the diffusional processes. Then, the addition of Ca^{2+} ions to the CO_3^{2-}/λ-Car solution could start the nucleation of calcium microcrystals not only by the carbonate anion on the polymer surface, but also by the λ-Car sulfonate groups. Even when the Kps of $CaCO_3$ is about 10^{-9}, several times lower than that of $CaSO_4$ salt (about 10^{-5}), the decreased diffusion of carbonate molecules in the solution may help the calcification process mediated by the sulfonate groups of λ-Car. Additionally, during the process of vaterite crystallization, the incorporation of the biopolymer into the $CaCO_3$ network be possible, as previously reported for Car and other polymers [12–14]. Evidence based on the hypothesis of biopolymer incorporation into the $CaCO_3$ matrix is the decrease in the hNP size compared with other microparticles composed of biopolymers and calcium carbonate alone (Fig. 2). Confocal microscopy of the cross section of hNPs and fluorescence microscopy analysis indicate that λ-Car was integrated not only on the particle surface, but also located inside the matrix of the hNPs (Figs. 3 and 4).

3.3. Microsphere surface and internal morphology

The diameter of the λ-Car-$CaCO_3$ microspheres (with and without FA) was *ca.* 2 μm by SEM analysis (Fig. 3), – with a relatively narrow size distribution (mean diameter, 2.5 ± 0.2 μm) – this dimension being about a half of that of the classical $CaCO_3$ (about 5 μm) (Supplemented Material, Fig. 1S). Surface analysis of the λ-Car microspheres indicated the presence of agglomerated vaterite nanograins similar to those previously reported (Fig. 3) [8]. The microparticle powder was slightly ground in a mortar and dispersed on an adhesive carbon support. A broken particle located and visualized by SEM (Fig. 3d, inset on the right) revealed that the environment inside the microspheres was homogeneous. No holes were present, but radial fibrous units around 1 μm in length were observed inside the microspheres. Thus, the growth of the $CaCO_3$ microcrystals within the particles was seen to be radial, as had been previously reported [14].

On the basis of matrix stability, because of the vaterite content along with the results displayed in the previous figures, the λ-Car-hNPs proved to be the best system owing to the high degree of homogeneity in terms of shape and size distribution. This system was therefore selected for further formulation studies.

3.4. Presence of biopolymer and stability in hNP systems

The FTIR and Raman spectra of the Cars recorded before and after hNP synthesis were not different. These results confirmed the integrity of the Cars during hNP gelation. Furthermore, no relevant interactions between the biopolymers and $CaCO_3$ were detected within the matrix, and no differences were observed in the integrity of the biopolymers present in the microparticles synthesized by different drying and washing processes. These results strongly suggested that the biopolymers were working as physical templates for $CaCO_3$ crystallization under those different experimental conditions. Finally, the Dox-loading capabilities of the hNPs were not compromised (data not shown).

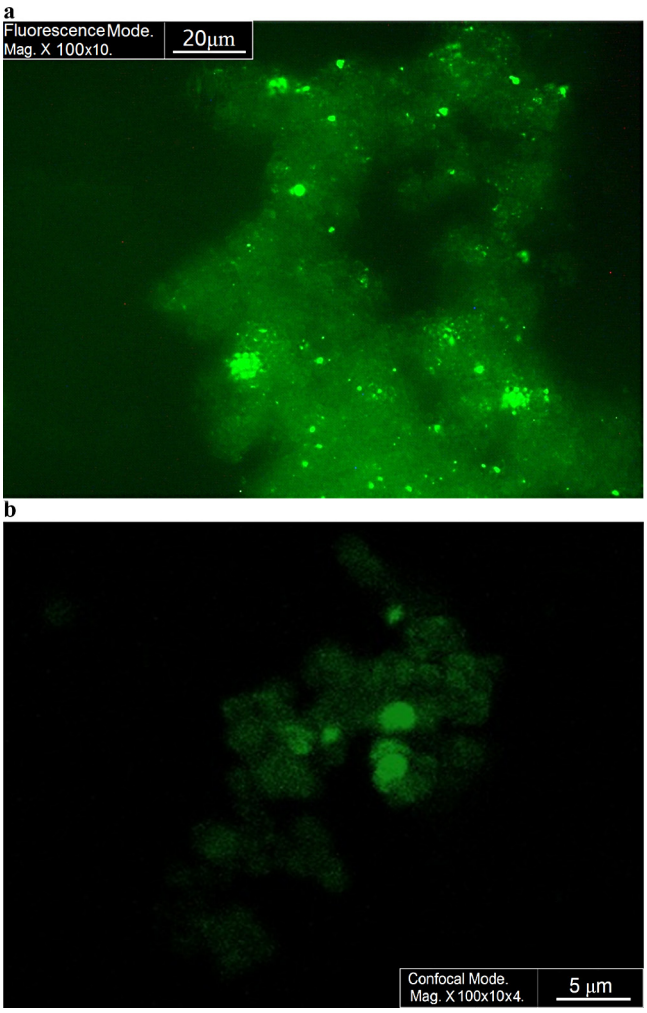

Fig. 4. λ-Car hNPs microscopies: (a) fluorescent and (b) confocal images.

The FITC-labeled λ-Car biopolymer was synthesized and added to the solution during hNP synthesis in order to confirm the presence and distribution of the biopolymer within the microparticles (Fig. 4). The images obtained by light and fluorescence microscopy were used to determine the presence and location of the labeled λ-Car within the microspheres (Fig. 4a and b), while flow-cytometry analysis was carried out to verify the presence of the labeled biopolymer within the isolated particles (data not shown). Confocal microscopy revealed that the biopolymer within the hNPs was both inside the microparticles and on the surface (Fig. 4).

The presence of λ-Car within the microspheres and the stability of the hybrid particles justified the choice of this system to be derivatized with FA. The FA molecule has the advantage of increasing the hydrophilicity of the λ-Car chains allowing the enhancement of Dox loading and release. Additionally, FA is one of the most recognized molecules used for cancer cell targeting.

3.5. Porosity determination by nitrogen adsorption

A porosity determination of the FA–λ-Car microspheres was carried out by N_2 adsorption and desorption at 77 K. Fig. 5a shows the isotherms obtained. Gas adsorption in the P/Po range of 0.1–0.3 gave a specific surface area of 27 $m^2\,g^{-1}$, as calculated by the BET equation (Fig. 5b), which was ninefold higher than previously reported for the $CaCO_3$ microspheres of a similar size range (1–2 μm) [27]. The high surface area compared to the 5-μm particle diameter can be explained by the presence of nanograins

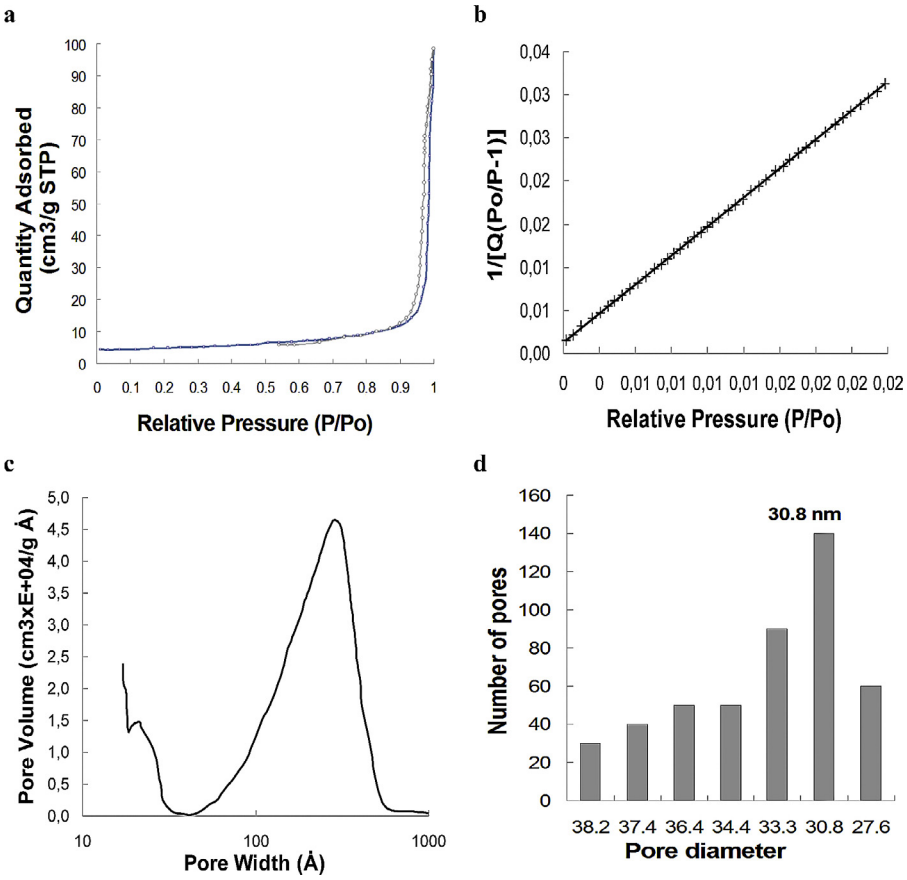

Fig. 5. Analysis of FA–λ-Car hNPs properties. (a) Nitrogen isotherms: adsorption (□) and desorption (○). (b) BET specific surface area analysis. (c) Volume pore determined by BJH. (d) Pore diameter of images obtained by SEM and estimated by ImageJ program.

agglomerated on the microsphere surface and by the internal porosity. In contrast to the synthesis under supercritical conditions, here the adsorption and desorption isotherms did not show a pronounced hysteresis at $P/P_0 > 0.43$ owing to the N_2-capillary condensation that takes place in the particle mesopores [8]. Moreover, the nanopores in the hNPs exhibited a low dispersion at around an average size of 30 nm (Fig. 5c and d), and these small dimensions of the nanopores could explain the increased Dox-loading capability for the λ-Car hNPs over that of the nanoparticles without Car that is indicated in the following sections.

3.6. Dox-loading studies

In order to maximize Dox encapsulation in the λ-Car hNP matrices, different loading processes and buffers were tested at various pHs (data not shown). The adsorption method for Dox loading at pH 6.5 in the presence of MES buffer under slow stirring at 4 °C for 6 h proved to be the best condition found. The presence of λ-Car in the hybrid systems provides some interaction with Dox expressed by moderate binding of the Dox molecules to the hybrid matrix compared with the non-hybrid microparticles. The experimental Dox loading values were 29% for λ-Car–$CaCO_3$ *versus* an undetectable amount of Dox in the $CaCO_3$ particles alone. The chemical derivatization of λ-Car with folic acid raised the Dox loading to 83% for FA–λ-Car–$CaCO_3$, which is about a threefold loading increase. The explanation for this big difference of the Dox loading in both matrices could be attributed to the increased number of polar residues, *e.g.*, carboxylate groups formed by the attachment of folic acid to Car, twice for each folic acid molecule incorporated to λ-Car, and also to the hydrophilic properties of the Dox molecule (log $P = 1.27$), which allowed increasing the drug loading and reducing the Dox release (see below) (Supplementary material, Fig. 2S).

3.7. Spectroscopy studies of the loading systems: FTIR analysis

The presence of λ-Car in the hNPs and the FA in the covalently modified biopolymer as well as the existence of vaterite as the main $CaCO_3$ polymorphism within the matrix were confirmed by FTIR analysis. The fact that FTIR revealed that the interaction between the λ-Car and Dox was as had been originally found by X-ray diffraction (Fig. 1) was reassuring.

Peaks characteristic of the λ-Car-hNPs were distinguished in the FTIR spectra (Fig. 6) representing the C=O stretching at 1690 cm^{-1}, the N—H bending at 1605 cm^{-1}, and the presence of the aromatic group at 1510 cm^{-1}. Moreover, an amide peak related to the binding of the biopolymer to FA was present at 1240 cm^{-1} [28].

In addition, the FTIR spectra of the Dox-loaded hNPs contained a characteristic Dox N—H peak that was shifted from 1615 cm^{-1} to 1628 cm^{-1} ($\Delta\nu = 13\ cm^{-1}$), while the 1722 cm^{-1} Dox carbonyl peak was displaced to 1733 cm^{-1} ($\Delta\nu = 11\ cm^{-1}$). The bands associated with the aromatic Dox motifs were also shifted from 1743 to 1733 cm^{-1} ($\Delta\nu = 10\ cm^{-1}$), suggesting a possible interaction with the hydrophobicity of the anthracycline aromatic ring.

Similarly, the λ-Car–Dox complex exhibited hypsochromic shifts within the σ_{C-C} vibrational mode compared to the underivatized-Dox spectrum [28]. Thus, these FTIR studies strongly suggested a complex interaction between the cargo and the matrix.

Finally, vaterite was detected in the FTIR spectra as the main $CaCO_3$ polymorph of the inorganic-matrix network (Fig. 7).

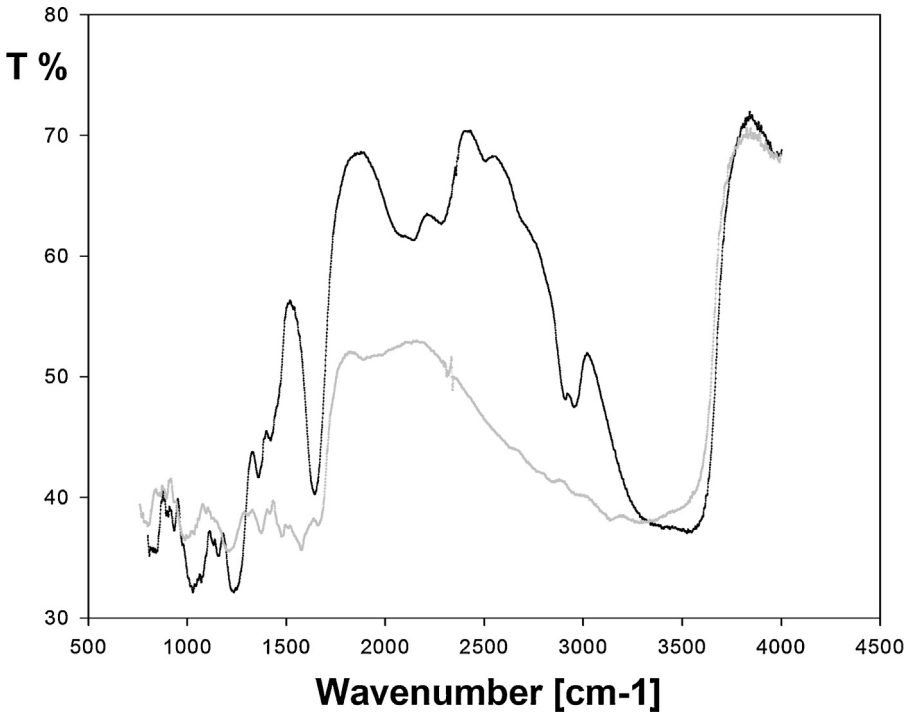

Fig. 6. FTIR spectra of λ-Car (▬) and FA–λ-Car (▬) used in the formulation of hNPs.

Simultaneous λ-Car–Dox-hNP analyses by fluorescent and light microscopy (Fig. 7a) coupled with FTIR-synchrotron spectroscopy (Fig. 7b) were performed on samples immobilized in an organic resin. A correlation was then established between the degree of Dox loading, inorganic stability, and the presence of the biopolymer in the matrix (Fig. 7).

Map analysis obtained from the synchrotron beam (Fig. 7b) indicated that the adsorption method developed for loading the particles with Dox had not affected the polymorphic stability of the hNPs because of the typical calcite peaks were absent from the FTIR spectra [29].

3.8. Dox-release studies

A kinetic analysis of Dox release was carried out on the λ-Car–Dox and FA–λ-Car–Dox hNPs, simulating the real physiologic conditions *in vivo* (*i.e.*, PBS buffer, 37 °C). After 5-day incubation, Dox release from the hNP matrix was not exhausted, but a plateau had been reached (Fig. 8). These kinetics can be explained by the strong interaction between the calcium ions and the λ-Car chains that produces a highly stable cross-linked gel. As a consequence, the Dox molecules were able to diffuse, though slowly, from the inner microsphere layers to the surface and then be released into the buffer. This release of Dox from the λ-Car–Dox hNPs was 73%, but from the derivatized FA–λ-Car–Dox hNPs it was only about a third as much, at 26%, after 25 days of incubation (Fig. 8).

3.9. Cell-culture assays

The cytotoxicity of hNPs to NIH-3T3 mouse fibroblasts was measured and compared to that of polystyrene microparticles of similar size after 96 h of incubation. No statistical differences were observed for the λ-Car and FA–λ-Car hNPs relative to the polystyrene control ($p < 0.01$; data not shown).

Supernatants of the FA–λ-Car–Dox microspheres were collected at different times and tested for cytotoxicity to the MG-63 human osteosarcoma cells. The crystal violet assay indicated a cell viability of 100%, 67%, 57%, and 36% in the cultures after 3, 6, 9, and 24 h of exposure to those hNP supernatants, respectively, relative to control cultures exposed to buffer alone (Fig. 9). The cell viability observed for different samples was in agreement with the Dox release from the FA–λ-Car–Dox hNPs (Fig. 8).

In addition, the hNPs' anticancer activity, when tested on the MG-63 cells, indicated a degree of cytotoxicity of FA–λ-Car–Dox hNPs similar to that seen with the Dox-containing supernatants, with the cultures exhibiting only 14% viability after 24 h of exposure to the Dox-laden microparticles. By contrast, when the hNPs contained no Dox in the control cultures, the cells remained 100% viable (Fig. 9). Similar cytotoxic effects to those observed here with the Dox-containing supernatants and hNPs were obtained when 30 μg/ml of Dox in the free state was added to the cultures. Furthermore, a significant increase in cytotoxicity was observed for both types of hNPs relative to the uncharged particles even after only 6 h ($p < 0.01$). Finally, non-stirred hNPs incubated with the cell line showed no decrease in cytotoxicity, but the cytotoxicity with the FA–λ-Car–Dox hNPs became more readily apparent at incubation times longer than 6 h.

4. Discussion

Microparticle synthesis depends on the physicochemical properties of the molecular medium as well as on the chemical components present in the solution, with both conditions playing a key role in the colloidal crystallization of salts. Consequently, biopolymers acting as templates determine the polymorphism of $CaCO_3$ crystals during hNP synthesis. On the basis of matrix stability owing to the vaterite content and degree of homogeneity in terms of size and shape, the λ-Car-HNPs system was therefore selected for further formulation studies.

FTIR and Raman spectroscopies along with X-ray diffraction indicated that hNPs containing Cars were stable systems exhibiting a high content of vaterite–$CaCO_3$ polymorphism analyzed after lyophilization. These results strongly suggested that the biopolymers were working as physical templates for the $CaCO_3$ nucleation

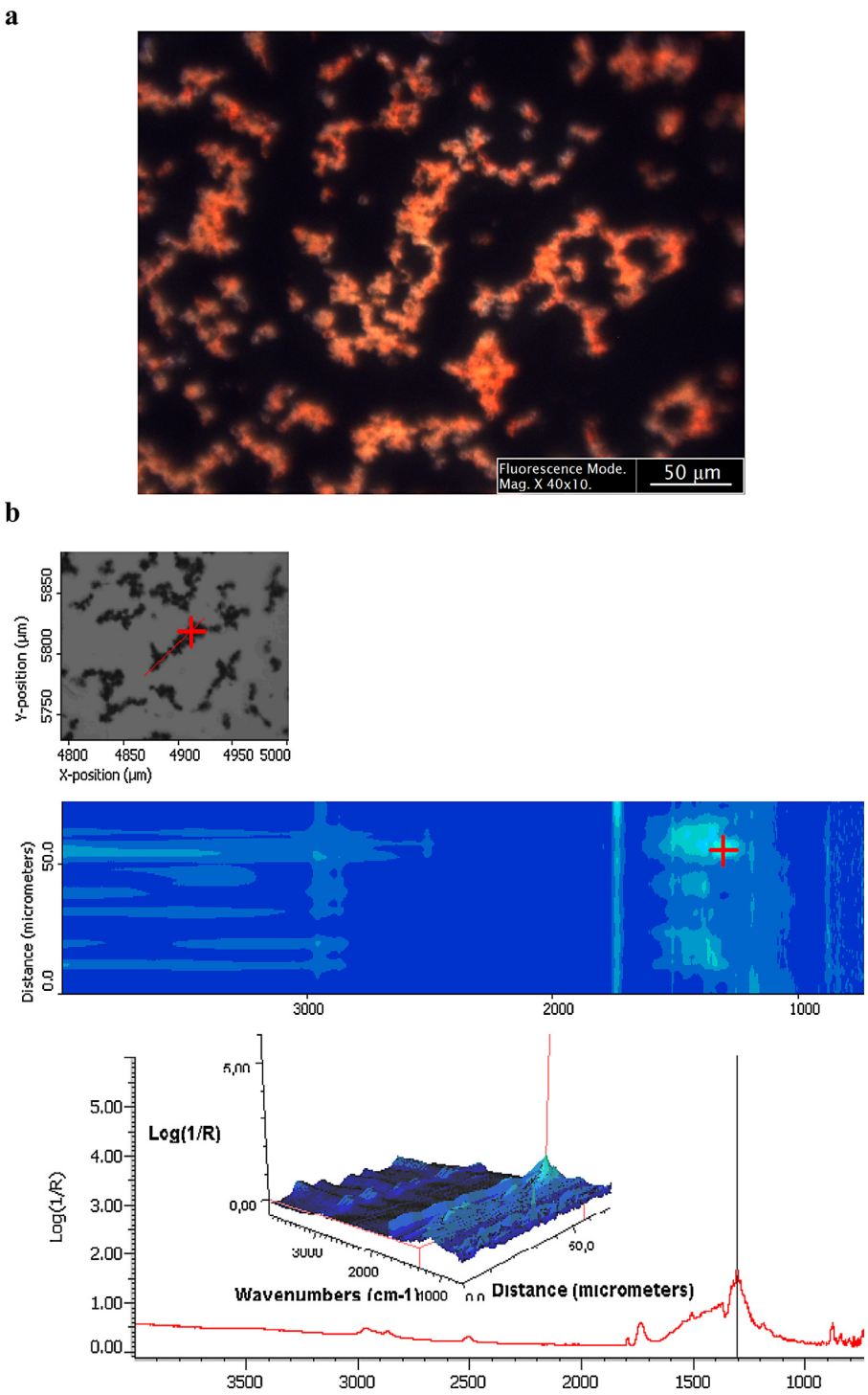

Fig. 7. Analysis of λ-Car–Dox hNPs by: (a) fluorescence microscopy; (b) FTIR synchrotron. Simultaneous λ-Car–Dox-hNP analyses by fluorescent, light microscopy and FTIR were performed on a cross section of samples immobilized in an organic resin.

under those different experimental conditions, where the Dox-loading capabilities of the hNPs were not compromised (data not shown).

Fluorescence spectroscopy and confocal microscopy revealed the presence of biopolymers in the porous inorganic matrix, while SEM indicated a homogeneous particle-size distribution. The smallest synthesized particles were Car hNPs compared to the classical $CaCO_3$ microparticles.

The presence of λ-Car within the microspheres and the stability of the hybrid particles justified the election of the system for targeting Dox to cancerous cells by FA. The tumor targeting of hNPs was thus performed by combining the λ-Car with folic acid (FA–λ-Car) as described in Section 2.

The results of the FTIR synchrotron-beam showed that the method of adsorption used in the Dox loading of the particles did not affect the stability of the hNPs in terms of the content of vaterite polymorphism. In addition, the presence of the biopolymer in the matrix increased the specific surface area of the material to up to ninefold (measured by the BET method) in the FA–λ-Car hNPs. The high surface area compared to the 5-µm particle diameter

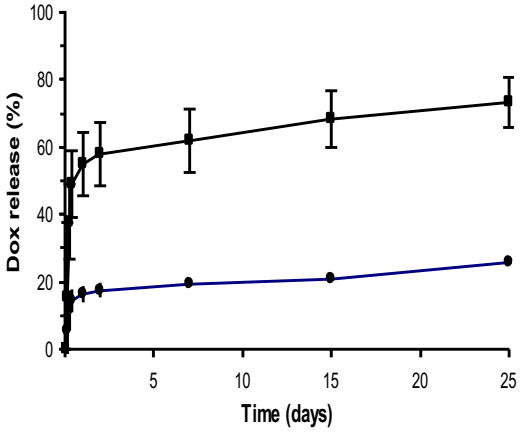

Fig. 8. Dox kinetic release profiles from λ-Car (■) and FA–λ-Car (●) hNPs. The values are the mean of three replicates ($n = 3$) with standard deviation (SD ≤ 10%). Differences among the data were assessed for statistical significance by analysis of variance (ANOVA) with a significance level of 5.0% ($p < 0.05$).

can be explained by the presence of nanograins agglomerated on the microsphere surface and by the internal porosity. The non-hysteresis can be attributed to the absence of a hollow core and could be related to the high stability of the vaterite network within the system during the Dox-loading process.

A nanostructured porous surface was found in all instances, with the FA–λ-Car-hNP pore size being about 30 nm (the Barrett–Joyner–Halenda adsorption average), and these small dimensions of the nanopores could explain the increased Dox-loading capability for the λ-Car HNPs over that of the nanoparticles without λ-Car.

The lyophilized Dox-loaded particles displayed a high stability as indicated by the percentages of vaterite and Dox released, and the FA–λ-Car-hNP system exhibited good loading capabilities. Moreover, FTIR studies of Dox loading strongly are suggesting a complex interaction between the cargo and the matrix.

A progressive sustained release was found under simulated physiologic conditions for λ-Car and FA–λ-Car hNPs in 25-day experiments. The anticancer activity tested on the human osteosarcoma cell line with FA–λ-Car hNPs indicated a higher cytotoxicity than with non-immobilized Dox.

A coalition of the strategies of controlled release and specific cell targeting in combination with hybrid biopolymeric-inorganic particles, as tested in the present model system, would appear to provide the means for a novel platform for cancer chemotherapy.

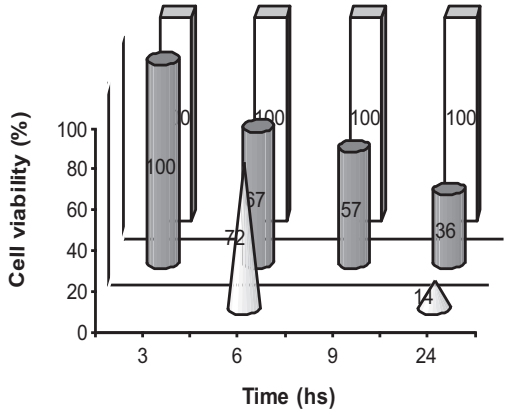

Fig. 9. Cell viability of MG-63 human osteosarcoma cell line. Symbols: (□), controls; (●), supernatants and (▲), hNPs of FA–λ-Car–Dox formulations.

Acknowledgements

The present work was supported by the Consejo Nacional de Investigaciones Científicas y Técnicas (CONICET, PIP0214), a CONICET-INSERM grant, and the Agencia Nacional de Promoción Científica y Técnica (PICT2011-2116) of Argentina. We wish to thank Dr. Paul Dumas (SMIS beamline, Soleil Synchrotron Facility, France) for his kind support and expertise during the sample analysis. We are also grateful to CPKelco (Buenos Aires, Argentina) for the gift of pectin and to Dr. Mario Malaspina and Dr. Natalio Kotliar from LKM Laboratories for the doxorubicin used in the present work. We gratefully acknowledge the financial support of ANR (France – Project ANR-09-PIRI-0004-01), the Regional Research program (Pays de Loire, France-Bioregos program), and the INSERM (France) and thank both IFREMER (Nantes, France) for characterization of the biopolymers by high-performance liquid chromatography and the SCIAM laboratory (Angers, France) for the SEM observations.

Appendix A. Supplementary data

Supplementary data associated with this article can be found, in the online version, at http://dx.doi.org/10.1016/j.colsurfb.2014.09.011.

References

[1] W.B. Liechty, D.R. Kryscio, B.V. Slaughter, N.A. Peppas, Polymers for drug delivery systems, Ann. Rev. Chem. Biomol. Eng. 1 (2010) 149.
[2] G.R. Castro, E. Bora, B. Panilaitis, D.L. Kaplan, Degradable polymers and materials, in: K. Khemani, C. Scholz (Eds.), American Chemical Society Symposium Series 939, Oxford University Press, Washington, 2006, p. 14.
[3] G. von Maltzahn, J.H. Park, K.Y. Lin, N. Singh, C. Schwöppe, R. Mesters, W.E. Berdel, E. Ruoslahti, M.J. Sailor, S.N. Bhatia, Nanoparticles that communicate in vivo to amplify tumour targeting, Nat. Mater. 10 (2011) 545.
[4] C. Peng, Q. Zhao, C. Gao, Sustained delivery of doxorubicin by porous $CaCO_3$ and chitosan/alginate multilayers-coated $CaCO_3$ microparticles, Colloids Surf. A 353 (2010) 132.
[5] V.E. Bosio, M.V. Machain, A. Gómez López, I.O. Pérez De Berti, S.G. Marchetti, M. Mechetti, G.R. Castro, Appl. Biochem. Biotechnol. 167 (2012) 1365.
[6] V.V. Glinsky, A. Raz, Modified citrus pectin anti-metastatic properties: one bullet, multiple targets, Carbohydr. Res. 344 (2009) 1788.
[7] V.L. Campo, D.F. Kawano, D. Braz da Silva Jr., I. Carvalho, Carrageenans: biological properties, chemical modifications and structural analysis – a review, Carbohydr. Polym. 77 (2009) 167.
[8] T. Beuvier, B. Calvignac, G. Delcroix, M.K. Tran, S. Kodjikian, N. Delorme, J.F. Bardeau, A. Gibauda, F. Boury, Synthesis of hollow vaterite $CaCO_3$ microspheres in supercritical carbon dioxide medium, J. Mater. Chem. 21 (2011) 9757.
[9] V.V. Hardikar, E. Matijević, Influence of ionic and nonionic dextrans on the formation of calcium hydroxide and calcium carbonate particles, Colloids Surf. A 186 (2001) 23.
[10] F.H. Shena, Q.L. Fenga, C.M. Wang, The modulation of collagen on crystal morphology of calcium carbonate, J. Cryst. Growth 242 (2009) 239.
[11] M. Díaz-Dosque, P. Aranda, M. Darder, J. Retuert, M. Yazdani-Pedram, J.L. Arias, E. Ruiz-Hitzky, Use of biopolymers as oriented supports for the stabilization of different polymorphs of biomineralized calcium carbonate with complex shape, J. Cryst. Growth 310 (2008) 5331.
[12] C. Kosanović, G. Falini, D. Kralj, Mineralization of calcium carbonates in gelling media, Cryst. Growth Des. 11 (2011) 269.
[13] M.R. Han, M.C. Kwon, H.Y. Lee, J.C. Kim, J.D. Kim, S.K. Yoo, I.S. Sin, S.M. Kim, pH-dependent release property of alginate beads containing calcium carbonate particles, J. Microencapsul. 24 (2007) 787.
[14] D. Volodkin, $CaCO_3$ templated micro-beads and -capsules for bioapplications, Adv. Colloid Interface Sci. 207 (2014) 306.
[15] O. Tacar, P. Sriamornsak, C.R. Dass, Doxorubicin: an update on anticancer molecular action, toxicity and novel drug delivery systems, J. Pharm. Pharmacol. 65 (2013) 157.
[16] I. Rodríguez-Ruiz, J.M. Delgado-López, M.A. Durán-Olivencia, M. Iafisco, A. Tampieri, D. Colangelo, M. Prat, J. Gómez-Morales, pH-Responsive delivery of doxorubicin from citrate-apatite nanocrystals with tailored carbonate content, Langmuir 29 (2013) 8213.
[17] S. Hossain, H. Yamamoto, E.H. Chowdhury, X. Wu, H. Hirose, A. Haque, Y. Doki, M. Mori, T. Akaike, Fabrication and intracellular delivery of doxorubicin/carbonate apatite nanocomposites: effect on growth retardation of established colon tumor, PLOS ONE 8 (4) (2013) e60428.
[18] S.A. Kamba, M. Ismail, S.H. Hussein-Al-Ali, T.A. Tengku Ibrahim, Z.A. Bakar Zakaria, *In vitro* delivery and controlled release of doxorubicin for targeting osteosarcoma bone cancer, Molecules 18 (2013) 10580.

[19] V.E. Bosio, A. Gómez López, A. Mukherjee, M. Mechetti, G.R. Castro, Tailoring doxorubicin sustainable release from alginate gel microspheres by carboxymethyl guar gum and Congo Red, J. Mater. Chem. B 2 (2014) 5178.
[20] G.T. Hermanson, Bioconjugate Techniques, 2nd ed., Academic Press, Waltham, 2008.
[21] Z. Zhaowu, Conjugating folic acid to gold nanoparticles through glutathione for targeting and detecting cancer cells, Bioorg. Med. Chem. 18 (2010) 5528.
[22] I.E. León, S.B. Etcheverry, B.S. Parajón-Costa, E.J. Baran, Spectroscopic characterization of an oxovanadium(IV) complex of oxodiacetic acid and o-phenanthroline. Bioactivity on osteoblast-like cells in culture, Biol. Trace Elem. Res. 147 (2012) 403.
[23] A.M. Cortizo, S.B. Etcheverry, Vanadium derivatives act as growth factor-mimetic compounds upon differentiation and proliferation of osteoblast-like UMR106 cells, Mol. Cell. Biochem. 145 (1997) 97.
[24] S.B. Etcheverry, D.C. Crans, A.D. Keramidas, A.M. Cortizo, Insulin-mimetic action of vanadium compounds on osteoblast-like cells in culture, Arch. Biochem. Biophys. 338 (1997) 7.
[25] S.R. Dickinson, K.M. McGrath, Quantitative determination of binary and tertiary calcium carbonate mixtures using powder X-ray diffraction, Analyst 126 (2001) 1118.
[26] M.E. Zabik, P.E. Aldrich, The effect of cations on the viscosity of lambda-carrageenan, J. Food Sci. 32 (1967) 91.
[27] J. Yu, W. Guo, S.A. Davis, S. Mann, Fabrication of hollow inorganic microspheres by chemically induced self-transformation, Adv. Funct. Mater. 16 (2006) 2035.
[28] D. Lin-Vien, N.B. Colthup, W.G. Fateley, J.G. Grasselli, The Handbook of Infrared and Raman Characteristic Frequencies of Organic Molecules, Academic Press, Boston, 1991.
[29] A. Andersen, D. Kralj, Determination of the composition of calcite-vaterite mixtures by infrared spectrophotometry, Appl. Spectrosc. 45 (1991) 1581.